Pure Appl. Geophys. 178 (2021), 1157–1164

https://doi.org/10.1007/s00024-021-02702-5

Pure and Applied Geophysics

The Effects of Variable and Constant Rupture Velocity on the Generation of High-Frequency Radiation from Earthquakes

Igor A. Beresnev[1] and Kaitlyn Roxby[1]

Abstract—A viewpoint exists that generation of seismic high frequencies results from sudden movements of ruptures, experiencing episodes of acceleration/deceleration. We investigated this effect theoretically for (1) the far field of a small near-line source and (2) the near field of a large fault computed exactly from the representation integral. The results indicate that, in both cases, the strength of the high-frequency radiation and the spectral fall-off for ruptures moving with constant positive or negative acceleration, as well as with regularly changing acceleration, are variable: depending on the parameters, they can exceed, be similar to, or fall below the levels produced by constant-velocity propagation. The directivity spectral levels for the scenarios of constant (positive or negative) acceleration, acceleration modulated by an orderly function, or constant velocity are fully controlled by regular interference: a particular high-frequency slope seen is an artifact of the case-specific interference. Randomization of rupture speed suppresses regular interference and creates an appearance of high-frequency generation by irregularity in the velocity, while in reality it is due to the elimination of artifacts. Realistic ruptures will always have a random component in their travel times, depending on fault and material properties, and will always exhibit elevated high-frequency content with respect to an idealized constant-velocity scenario. The conclusion is that interpreting this phenomenon as high-frequency generation by rupture irregularity would be incorrect. The additional ω^{-1} spectral roll-off, typically attributed to fault finiteness, is a consequence of the constant-velocity assumption. Removing the latter flattens the spectrum, even for a finite fault.

Keywords: Earthquake radiation, ground motions, representation theorem, rupture propagation.

1. Introduction

An opinion can be found in the literature that enrichment of seismic radiation in high frequencies is a result of acceleration or deceleration of ruptures (Madariaga 1977, 1983; Somerville et al. 1999, p. 60; Shi and Day 2013). One can turn to the representation theorem of elasticity to evaluate the theoretical basis for this viewpoint. The representation integral prescribes the exact wave field radiated by a displacement discontinuity across a fault surface in an elastic space (Aki and Richards 1980, their Eq. 14.37). For a slip ("source time") function in the form of a radially propagating rupture,

$$\Delta u(\xi, t) = U(\xi)\Delta u(t - r/v), \tag{1}$$

where $U(\xi)$ is the distribution of final-slip values over the fault plane, r is the distance from the hypocenter, and v is the rupture-propagation speed, the Fourier transform of the ith component of the radiated displacement field $u_i(\mathbf{x}, t)$ is

$$\begin{aligned} &u_i(\mathbf{x},\omega) \\ &= \frac{\mu}{4\pi\rho}\Delta u(\omega)\iint U(\xi)e^{-i\omega\frac{r}{v}}\left[\frac{30\gamma_i n_p\gamma_p\gamma_q v_q - 6v_i n_p\gamma_p - 6n_i\gamma_q v_q}{R^4}t_1(\omega)\right. \\ &+\frac{12\gamma_i n_p\gamma_p\gamma_q v_q - 2v_i n_p\gamma_p - 2n_i\gamma_q v_q}{\alpha^2R^2}e^{-i\omega\frac{R}{\alpha}} \\ &-\frac{12\gamma_i n_p\gamma_p\gamma_q v_q - 3v_i n_p\gamma_p - 3n_i\gamma_q v_q}{\beta^2R^2}e^{-i\omega\frac{R}{\beta}} + \frac{2\gamma_i n_p\gamma_p\gamma_q v_q}{\alpha^3R}i\omega e^{-i\omega\frac{R}{\alpha}} \\ &\left.-\frac{2\gamma_i n_p\gamma_p\gamma_q v_q - v_i n_p\gamma_p - n_i\gamma_q v_q}{\beta^3R}i\omega e^{-i\omega\frac{R}{\beta}}\right]d\Sigma(\xi), \end{aligned} \tag{2}$$

$$t_1(\omega) = \frac{1}{\omega}\left[e^{-i\omega\frac{R}{\beta}}\left(i\frac{R}{\beta}+\frac{1}{\omega}\right) - e^{-i\omega\frac{R}{\alpha}}\left(i\frac{R}{\alpha}+\frac{1}{\omega}\right)\right] \tag{3}$$

(Beresnev 2017a, Eqs. 4, 5). Here $\mathbf{x}$ and ξ are the coordinates of the observation point and the point on the fault surface, respectively, $\mathbf{n}$ is the unit vector in the direction of slip, $\mathbf{v}$ is the unit normal pointing from the side Σ^- of the fault to Σ^+, $R = |\mathbf{x} - \xi|$, $\boldsymbol{\gamma} = (\mathbf{x} - \xi)/R$, α and β are the P- and S-wave speeds, and μ and ρ are the shear modulus and density of the

[1] Department of Geological and Atmospheric Sciences, Iowa State University, 253 Science I, 2237 Osborn Drive, Ames, IA 50011-3212, USA. E-mail: beresnev@iastate.edu

medium. Also, $\Delta u(\omega)$ is the Fourier transform of $\Delta u(t)$. The double integration is carried over the fault plane $\Sigma(\boldsymbol{\xi})$.

Equation (2) assumes that the temporal shape of the source time function $\Delta u(t)$ is the same at all points on the fault. It shows that the spectrum of the seismic field is that of the source time function $\Delta u(\omega)$ modified by a frequency- and station-azimuth dependent integral $\mathbf{I}(\mathbf{x},\omega)$ over the fault plane representing the fault's directivity pattern,

$$\mathbf{u}(\mathbf{x},\omega) = \Delta u(\omega)\mathbf{I}(\mathbf{x},\omega). \tag{4}$$

We will refer to $\mathbf{I}(\mathbf{x},\omega)$ as the directivity spectrum. The presence of $\mathbf{I}(\mathbf{x},\omega)$ as the surface integral in (2) is purely due to the fault finiteness. When the source dimensions shrink to a point, all distance-dependent factors are taken out of the integral, and $u_i(\mathbf{x},\omega)$ converges to the classic expression for the radiation from a point shear dislocation (Aki and Richards 1980, their Eq. 4.32).

The classic "ω-squared" far-field spectral shape comes from the spectrum of the source time function $\Delta u(\omega)$ (Beresnev and Atkinson 1997, their Eq. 11; Beresnev 2019a, his Eq. 6). Any modification to the high-frequency roll-off in the ω-squared model is due to the $\mathbf{I}(\mathbf{x},\omega)$ term as the finite-fault effect.

The integral can be generalized to the case of rupture propagation with variable velocity by replacing the time delay r/v in Eq. (1) by a fault-position dependent $\Delta t(r)$ of arbitrary form. The $\exp(-i\omega r/v)$ multiplier before the brackets in the integrand of (2) will then become $\exp[-i\omega\Delta t(r)]$. Modified this way, the directivity integral $\mathbf{I}(\mathbf{x},\omega)$ can be analyzed for the effect of accelerating/decelerating rupture on radiation, relative to the constant-velocity case. To verify if variable velocity will consistently produce enhanced high-frequency content in seismic waves, we will consider the following scenarios: (1) a rupture traveling with constant acceleration, (2) rupture with constant deceleration, (3) the velocity changing periodically, and (4) the velocity containing a random component. We will analyze the full integral in (2), as well as its simplified asymptotic form allowing analytical solution.

Kinematic characterization of extended-source properties involving both constant and variable rupture-speed scenarios is an important component of modern large-scale numerical simulations of earthquake hazards (Graves and Pitarka 2010, their Figs. 2 and 9; Infantino et al. 2020, pp. 2563–2564; Rodgers et al. 2020, their Fig. 2). Understanding the physical causes of the differences in the radiated high-frequency energy between the two scenarios is acquiring substantial practical relevance.

2. *Far Field of Unidirectional Near-Line Source*

In the limits of (1) a near-line source with small width W, extending to the length L along the coordinate ξ_1, (2) small source dimensions, and (3) the far field, for the rupture traveling along ξ_1 with constant velocity, the modulus of the directivity spectrum $|\mathbf{I}(\mathbf{x},\omega)|$ reduces to

$$\begin{aligned}|\mathbf{I}(\mathbf{x},\omega)| &= \omega W\left|\int_0^L \exp\left[i\omega\left(\frac{\xi_1}{v}-\frac{\xi_1\cos\Psi}{c}\right)\right]d\xi_1\right| \\ &\equiv \omega W|\mathbf{I}_1(\mathbf{x},\omega)|,\end{aligned} \tag{5}$$

where c is either the P- or S-wave propagation speed, and Ψ is the angle between the direction to the receiver and the axis ξ_1 (Aki and Richards 1980, their Eq. 14.18) [Aki and Richards omit the dimensional multiplier $\mu/(4\pi\rho c^3 R)$ in their equation, which is also omitted from (5)].

For a variable rupture velocity, the time delay ξ_1/v in the integrand of (5) should be replaced by a spatially variable $\Delta t(\xi_1)$, leading to the integral

$$\mathbf{I}_1(\mathbf{x},\omega) = \int_0^L \exp\left\{i\omega\left[\Delta t(\xi_1)-\frac{\xi_1\cos\Psi}{c}\right]\right\}d\xi_1. \tag{6}$$

2.1. *Accelerating/Decelerating Rupture*

The time for a rupture, starting with the velocity v_0 and accelerating/decelerating with constant acceleration a, to reach a distance ξ_1 is

$$\Delta t(\xi_1) = \frac{-v_0 + \sqrt{v_0^2 + 2a\xi_1}}{a}. \tag{7}$$

Substitution of Eq. (7) into (6) yields the directivity spectrum of the unidirectional near-line source for an accelerating/decelerating rupture. The integral can be evaluated analytically, with the result (for $a > 0$)

$$\mathbf{I}_1(\mathbf{x},\omega) = \frac{ic\sqrt{\frac{\pi}{\cos\Psi}\frac{\omega}{\omega_{01}}}}{2\omega\cos\Psi} e^{\frac{i}{2\cos\Psi}\frac{\omega}{\omega_{01}}} \left\{ -\frac{2e^{-\frac{i}{2\cos\Psi}\frac{\omega}{\omega_{01}}}}{\sqrt{\frac{\pi}{\cos\Psi}\frac{\omega}{\omega_{01}}}} \left(1 - e^{-i\cos\Psi\frac{\omega}{\omega_{02}}} e^{i\sqrt{2}\frac{\omega}{\omega_{03}}}\right) \right.$$
$$+ (1-i)\,\mathrm{erfi}\left[\left(\frac{1}{2} - \frac{i}{2}\right)\sqrt{\frac{1}{\cos\Psi}\frac{\omega}{\omega_{01}}}\right]$$
$$\left. -\sqrt{-2i}\,\mathrm{erfi}\left[\left(\frac{1}{2} - \frac{i}{2}\right)\left(\sqrt{\frac{1}{\cos\Psi}\frac{\omega}{\omega_{01}}} - \sqrt{2\cos\Psi\frac{\omega}{\omega_{02}}}\right)\right]\right\}, \tag{8}$$

where three characteristic frequencies,

$$\omega_{01} = \frac{a}{c},\ \omega_{02} = \frac{c}{L},\ \omega_{03} = \sqrt{\frac{a}{L}}, \tag{9}$$

have been introduced. Here $\mathrm{erfi}(z)$ is the imaginary error function, $\mathrm{erfi}(z) = \mathrm{erf}(iz)/i$, and $\mathrm{erf}(z)$ is the error function, $\mathrm{erf}(z) = (2/\sqrt{\pi})\int_0^z \exp(-t^2)dt$. For the compactness of the expressions, $v_0 = 0$ (rupture initially at rest) has been assumed.

As an example, the modulus of Eq. (8) for $\Psi = 0$ is

$$|\mathbf{I}_1(\omega)| = \frac{c}{2}\sqrt{\frac{\pi}{\omega\omega_{01}}}\sqrt{\frac{8\sin\theta_1}{\sqrt{\pi\frac{\omega}{\omega_{01}}}}\left[\frac{2\sin\theta_1}{\sqrt{\pi\frac{\omega}{\omega_{01}}}} - (a_1 - a_2)\sin\theta_2 - (b_1 - b_2)\cos\theta_2\right] + (a_1 - a_2)^2 + (b_1 - b_2)^2}, \tag{10}$$

where the following notation has been used:

$$\theta_1 = \frac{\frac{\omega}{\omega_{02}} - \sqrt{2}\frac{\omega}{\omega_{03}}}{2}, \theta_2 = \frac{1}{2}\frac{\omega}{\omega_{01}} + \theta_1,$$
$$(1-i)\mathrm{erfi}\left[\left(\frac{1}{2} - \frac{i}{2}\right)\sqrt{\frac{\omega}{\omega_{01}}}\right] \equiv a_1 + ib_1, \tag{11}$$
$$\sqrt{-2i}\,\mathrm{erfi}\left[\left(\frac{1}{2} - \frac{i}{2}\right)\left(\sqrt{\frac{\omega}{\omega_{01}}} - \sqrt{2\frac{\omega}{\omega_{02}}}\right)\right] \equiv a_2 + ib_2.$$

For comparison, the directivity spectrum for a rupture traveling with constant velocity, obtained as the integral in (5), is

$$|\mathbf{I}_1(\mathbf{x},\omega)| = L\left|\frac{\sin X}{X}\right|, \tag{12}$$

where $X = (\omega L/2)[1/v - (\cos\Psi)/c]$ (Aki and Richards 1980, their Eq. 14.18).

One can see that Eq. (10) (accelerating rupture) is much more complex in form than Eq. (12) (constant speed) and allows a wide variety of frequency behaviors, depending on the interplay between the three frequency scales (9). In the following example, the rupture starts at $\xi_1 = 0$ with zero velocity and reaches a terminal velocity v_t at $\xi_1 = L$. The acceleration consequently is $a = (v_t^2 - v_0^2)/(2L) = v_t^2/(2L)$. Equation (10) was evaluated for the shear-wave radiation ($c = \beta$) for a fault with the length L = 3400 m, corresponding approximately to an M_w = 5 earthquake (Wells and Coppersmith 1994, table 2A). The shear-wave velocity was chosen as $\beta = 5000/\sqrt{3}$ m/s.

Figure 1 compares the directivity spectra of shear-wave radiation $|\mathbf{I}_1(\omega)|$ between a constant-velocity (black line) and accelerating (gray lines) ruptures. The former was calculated from Eq. (12) (for $\Psi = 0$: radiation in the direction of rupture propagation) with $v = 0.5\beta$. The latter were computed from Eqs. (10), (11) for three values of terminal velocities, $v_t = 0.5\beta$, 0.8β, and β as labeled. The conclusion drawn from this example is that the frequency fall-off in the radiation produced by an accelerating rupture is variable, leading to the strength of high frequencies

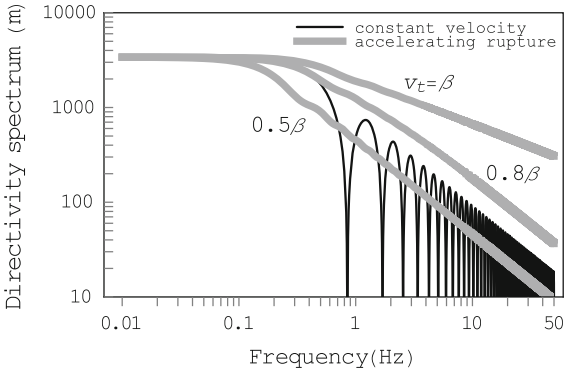

Figure 1
Comparison of the directivity spectra of shear-wave radiation from a near-line source between a constant-velocity (black line) and accelerating (gray lines) ruptures. Three terminal velocities are considered for the acceleration case, as labeled; the initial velocity is always zero

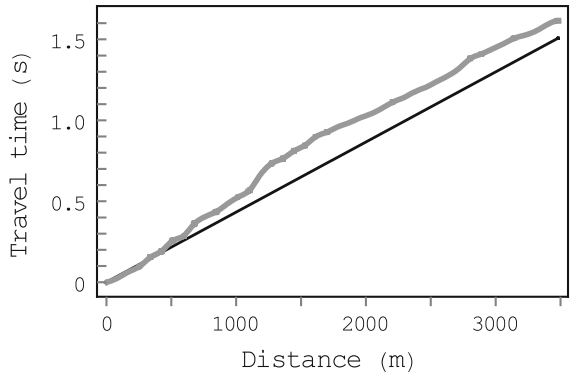

Figure 2
Rupture-propagation times along the near-line fault for the constant and randomized velocities

that can be above, similar to, or below the level produced by constant-velocity propagation, depending on the parameters.

The reverse scenario of a decelerating rupture, in which the starting and terminal velocities switched, the acceleration keeping the same absolute value but acquiring the negative sign, led to the amplitude spectra identical to those for the respective acceleration case, for any Ψ.

It would therefore be erroneous to conclude that rupture acceleration/deceleration always produces high-frequency content that is stronger than that for a constant velocity.

2.2. *Rupture with Randomized Speed*

The envelope of the directivity spectrum (12) of constant-velocity rupture, representing a sinc function, always has the ω^{-1} spectral roll-off. Aki and Richards (1980, p. 808) attributed the first discussion of this result to Ben-Menahem (1961) as the classic effect of fault finiteness on the radiated amplitude spectrum. One can argue that the condition of constant rupture speed is idealized and probably never materializes in reality: it would therefore be worth asking the question whether the same phenomenon holds if the velocity is slightly disturbed. To this end, Beresnev (2019b) produced a spatially variable travel time $\Delta t(\xi_1)$ in (6) to contain a normally distributed random variable η with zero

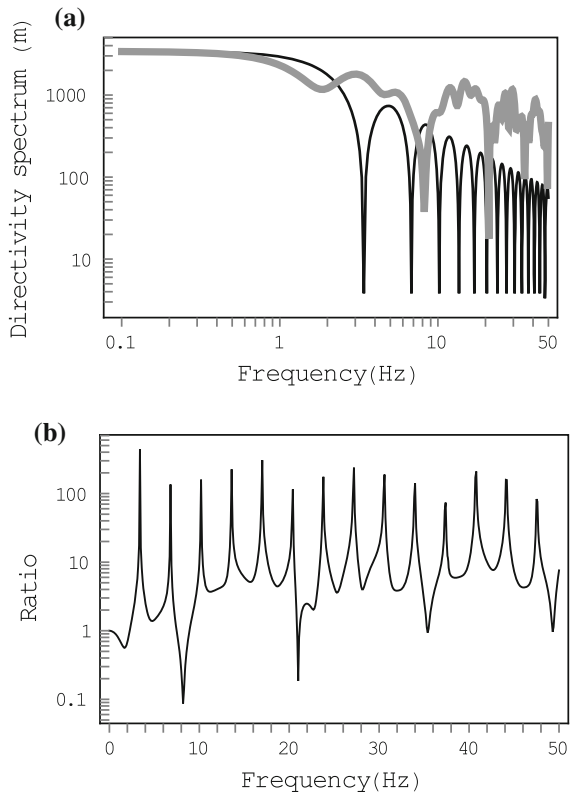

Figure 3
a Comparison of the directivity spectra of shear-wave radiation from a near-line source for the cases of constant and randomly perturbed rupture velocities (black and gray lines, respectively). **b** The ratio between the gray and black lines in **a**

mean and standard deviation of 0.3, modulating the constant velocity v as $v(1+\eta)$. The value of v was chosen as 0.8β. The fault length and β still were $L = 3400$ m and $\beta = 5000/\sqrt{3}$ m/s. Both the

constant-velocity and randomized travel-time curves are shown in Fig. 2. The integral (6) was then evaluated numerically.

Figure 3a compares the directivity spectra of shear-wave radiation $|\mathbf{I}_1(\omega)|$ for the cases of constant (black line) and randomized (gray line) rupture speeds and $\Psi = 0$ (Beresnev 2019b). The constant-velocity scenario was calculated from Eq. (12). Figure 3b is the ratio between the gray and black lines. A notable difference is that, while the constant-speed spectrum is the sinc function, the one for the randomized velocity is nearly flat and has the level of high frequencies that is about an order of magnitude stronger on average. A similar result was obtained by Boore and Joyner (1978, their Fig. 7).

One could be tempted to conclude that the apparent high-frequency generation in the case of randomized velocity is a consequence of the "jerkiness" in the rupture process, resulting in uneven velocity as seen in Fig. 2. In reality, the steeper fall-off is the result of the assumption of constant v, producing an artifact of regular pattern of destructive interference with the shape of a sinc function (Boore and Joyner 1978; Aki and Richards 1980, p. 810). Randomness in the timing of rupture at different parts of the fault suppresses the regular interference, nearly eliminating the additional slope. The resulting apparent enhancement in the high-frequency content is not the consequence of suddenly accelerating or decelerating rupture, but is the result of the elimination of the artifact. The conclusion again is that it is not the variable rupture speed that produces the elevated high-frequency content, but rather that the idealized assumption of constant speed artificially suppresses the high frequencies. The classic notion that fault finiteness necessarily leads to the additional ω^{-1} high-frequency slope is not true, once the constant-velocity condition is removed.

3. Near Field of a Finite Fault

The conclusions so far have been drawn from a simplified model of a small near-line source radiating into the far field. The directivity spectrum $\mathbf{I}(\mathbf{x}, \omega)$ in Eq. (4) then allows analytical solution. We now wish to verify whether the same inferences hold for the full seismic field described by Eqs. (2), (3). This general case will not involve any limiting assumptions on the source size or the distance to the observation point. To this end, the full surface integral $\mathbf{I}(\mathbf{x}, \omega)$, as defined in (2)–(4), was evaluated numerically for the fault-normal component of the seismic displacement with the precision of three digits. The $\exp(-i\omega r/v)$ multiplier before the brackets in the integrand of (2) was replaced with the distance-dependent $\exp[-i\omega\Delta t(r)]$ as applicable to the particular scenario considered. Calculations were performed for a 3400 × 3400 m vertical right-lateral strike-slip fault, for which the geometric coefficients $\gamma_i n_p \gamma_p \gamma_q v_q$, $v_i n_p \gamma_p$, and $n_i \gamma_q v_q$ in (2) reduce to simple analytical forms (Beresnev 2017b, Eqs. 7). The observation point was 200 m above the upper corner of the fault and offset by 200 m in the direction perpendicular to the fault plane, as shown in Fig. 1 of Beresnev (2017a). The hypocenter was placed in the center of the fault. A constant final slip $U(\boldsymbol{\xi}) = U_0$ over the fault plane was assumed. The value of U_0 = 0.14 m was derived from the magnitude (M_w = 5) by combining the definitions of the seismic moment, $M_0 = \mu U_0 A$, where A is the fault area, and of the moment magnitude, $M_w = (2/3)\log M_0 - 10.7$. The values of $\alpha = 5000$ m/s, $\beta = 5000/\sqrt{3}$ m/s, $\rho = 2700$ kg/m^3, and $\mu = \beta^2\rho$ were used.

Five scenarios of variable-velocity function were considered. In the first two, the rupture travels with a constant positive or negative acceleration. The function $\Delta t(r)$ is then described by Eq. (7), where ξ_1 is replaced by r. As in the example of Fig. 1, the rupture starts at $r = 0$ (the hypocenter) with zero velocity and travels with constant acceleration to reach a terminal velocity at the corners of the fault. The terminal velocity was β. For the deceleration case, the terminal and starting velocities reversed positions.

The third case involved the velocity spatially modulated by a sinusoidal function, representing periods of faster and slower movement with variable acceleration,

$$v(r) = \overline{v} + v_a \sin kr, \tag{13}$$

where the value of the constant $\overline{v}$ was 0.5β, the amplitude v_a was $0.75\overline{v}$, and the spatial period $2\pi/k$ was 100 m. The travel time to distance r under this velocity law is found as

$$\Delta t(r) = \int_0^r \frac{dr}{v(r)} = \int_0^r \frac{dr}{\bar{v} + v_a \sin kr}$$
$$= \frac{2}{k\sqrt{\bar{v}^2 - v_a^2}} \left(\arctan \frac{v_a + \bar{v} \tan \frac{kr}{2}}{\sqrt{\bar{v}^2 - v_a^2}} - \arctan \frac{v_a}{\sqrt{\bar{v}^2 - v_a^2}} \right). \quad (14)$$

The function (14) oscillates between $\left[2/\left(k\sqrt{\bar{v}^2 - v_a^2}\right)\right]\left[-\pi/2 - \arctan\left(v_a/\sqrt{\bar{v}^2 - v_a^2}\right)\right]$ and $\left[2/\left(k\sqrt{\bar{v}^2 - v_a^2}\right)\right]\left[\pi/2 - \arctan\left(v_a/\sqrt{\bar{v}^2 - v_a^2}\right)\right]$ with the full swing of $2\pi/\left(k\sqrt{\bar{v}^2 - v_a^2}\right)$ and the period of $kr/2 = \pi$. The periodicity is the required mathematical behavior to keep the arctangent a unique function of r. Physically, the travel time cannot oscillate and can only increase with distance. To achieve the required physical behavior, the function (14) should be corrected: every time $\tan(kr/2)$ enters the new period, other than first, the value of $2\pi/\left(k\sqrt{\bar{v}^2 - v_a^2}\right)$ should be added to the travel time. Such corrected behavior is achieved by adding a term to Eq. (14):

$$\Delta t_{corr}(r) = \Delta t(r) + \frac{2\pi}{k\sqrt{\bar{v}^2 - v_a^2}} \text{ round } \frac{\frac{kr}{2}}{\pi}, \quad (15)$$

where round (x) is the rounding function, giving the integer closest to x. In the term round$[(kr/2)/\pi]$, therefore, the values of $kr/2$ below $\pi/2$ are rounded to zero, the values between $\pi/2$ and $3\pi/2$ to one, the values between $3\pi/2$ and $5\pi/2$ to two, etc.

In the fourth scenario, the rupture travels with a constant velocity of 0.8β with a random component added to $\Delta t(r)$. The randomization was performed in the same way as in the example of Fig. 2. Finally, the fifth and sixth scenarios were for the constant travel speeds, $v = 0.5\beta$ and 0.8β.

The travel-time curves for all six cases are depicted in Fig. 4a, where r extends from zero to the distance from the center to the corners of the fault. Equation (15) was used for the term $\Delta t(r)$ in the third scenario.

Figure 4b presents the moduli of the directivity spectra $|\mathbf{I}(\mathbf{x}, \omega)|$, evaluated numerically from the full integral defined in (2)–(4) for all six rupture-propagation cases. The first conclusion drawn from

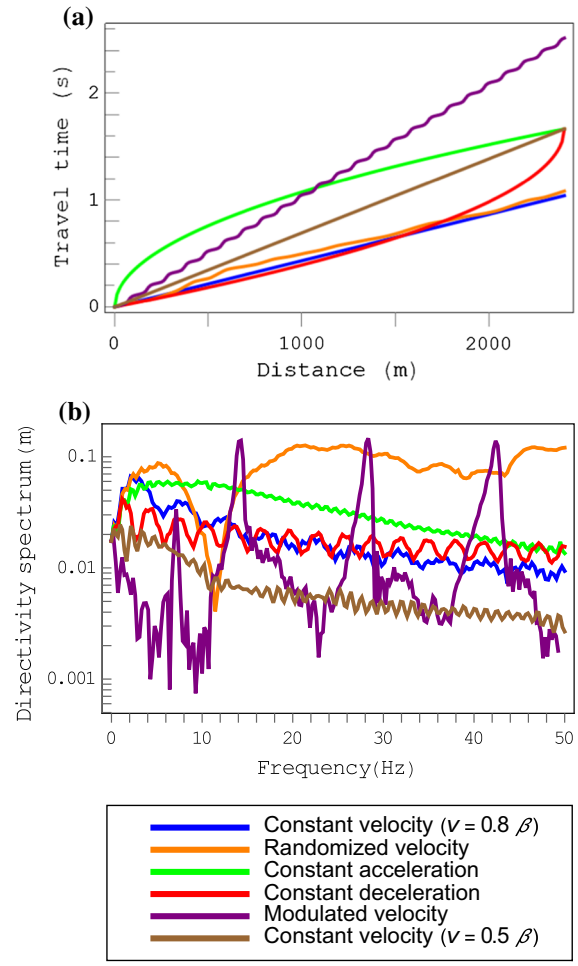

Figure 4
a Rupture-propagation times along the finite fault for various constant and variable rupture-velocity scenarios. **b** The near-field directivity spectra corresponding to each scenario

examining the curves is similar to what one previously learnt from the model of the line source: the strength of the high-frequency radiation and the high-frequency slope are primarily dictated by the interference pattern for the particular velocity law. The variable-velocity cases, in which rupture is accelerating, decelerating, or undergoing both, are not necessarily causing an elevated high-frequency content with respect to the constant-velocity cases. For example, the deceleration case (red line) and that of the constant $v = 0.8\beta$ (blue line) produce nearly same high-frequency levels. The spectrum for the modulated velocity (purple line) is low except for the pronounced peaks that are equally spaced and are a

product of the periodic velocity law (13). Also, the cases of the constant acceleration that has the same modulus but different sign (green and red lines) produce different spectra, whereas the latter were the same for the line source. The identical spectra for the line source are a consequence of the simplifications made in deriving the approximate far-field expression (5), in which the angle Ψ is assumed constant for any point along the length of the fault, causing the source to effectively collapse to a point. This is no longer true for the fault of finite dimensions.

Similarly to the line source, a notable exception is the randomized-velocity scenario, in which the directivity spectrum (orange line) is conspicuously stronger than any other curve in Fig. 4b. Its ratio to the respective constant-velocity curve (the ratio between the orange and blue lines) is presented in Fig. 5. The effect of randomization on boosting the high-frequency content has the same order of magnitude as for the line source (cf. Fig. 3b), on average. As for the line source, the high-frequency slope for any other case is an artifact of the particular case-specific interference pattern. Once the artifacts due to the regularity in the velocity law are removed, the radiation becomes uniformly stronger. As in the case of the line source, this phenomenon is not a consequence of the sudden movements of rupture, but rather of the elimination of the artificially imposed restriction. Attributing it to rupture acceleration/deceleration would be incorrect.

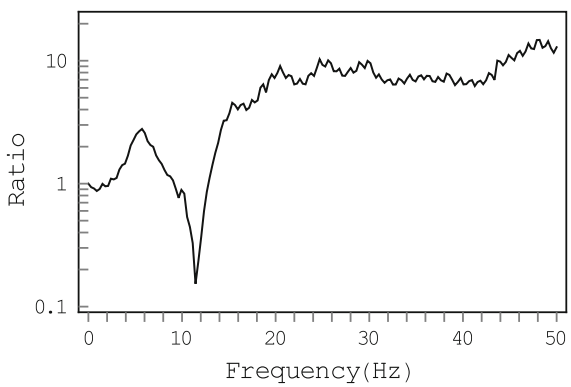

Figure 5
The ratio between the directivity spectra for the randomized velocity and constant $v = 0.8\beta$ (orange to blue lines) in Fig. 4b

Small-scale oscillations are seen in the spectra in Fig. 4b, except in the random case. These are the product of orderly interference due to a regularity in the velocity law. As expected, the oscillations disappear when randomness suppresses interference, as in the analogous comparison between the constant- and randomized-velocity cases for the line source in Fig. 3a.

4. Conclusions

Variable velocity (rupture acceleration/deceleration) in itself is not a sustaining source of high frequencies in the radiated seismic spectra, compared to constant velocity, as is frequently thought. If an ordered (regularly changing with distance) velocity function is used, the emitted spectra are controlled by the interference effects. The effect on the spectral slope is variable, depending on the parameters, but a gradual spectral decay at high frequencies is typically preserved as an artifact. If the velocity function becomes disordered, with a stochastic component superimposed, the regular interference is suppressed, creating an appearance of high-frequency generation, while in reality this is caused by the elimination of artifacts. A realistic rupture can be expected to always have a random component in its velocity, depending on natural variations in fault and rock properties along its way. It will therefore radiate a greater high-frequency content than an idealized model with a regular change in velocity. This conclusion has been drawn for both an asymptotic small near-line source observed in the far field and a general source of finite dimensions without any restrictions on the size of the fault plane or distance to the receiver.

The effect of fault finiteness does not necessarily lead to the extra negative power in the spectral decay with frequency, as also is often assumed, as long as there is a random component in the rupture velocity.

While the directivity effects on fault's radiation can be variable, the spectrum of the source-time function $\Delta u(\omega)$ is always present as a multiplier in the full spectrum of the emitted field (Eq. 4) and is thus the main controlling factor in determining the strength of the high-frequency content. As was

directly verified by Beresnev (2017a) by the numerical integration of Eqs. (2), (3), the fault-slip heterogeneity is not a significant factor either. Specifically, randomly disturbing the uniform slip and the maximum slip rate or introducing asperities did not lead to any appreciable differences in the shape of radiated Fourier spectra.

Acknowledgements

Constructive anonymous-review comments are appreciated.

Funding

Not applicable.

Availability of data and material

No data were used in the paper. All inferences were made through the analyses of the respective equations and literature sources as indicated.

Declarations

Conflicts of interest All author(s) declare that they have no conflict of interest.

Publisher's Note Springer Nature remains neutral with regard to jurisdictional claims in published maps and institutional affiliations.

References

Aki, K., & Richards, P. G. (1980). *Quantitative Seismology*. W. H. Freeman and Company.

Ben-Menahem, A. (1961). Radiation of seismic surface waves from finite moving sources. *Bulletin of the Seismological Society of America, 51,* 401–435.

Beresnev, I. A. (2017a). Factors controlling high-frequency radiation from extended ruptures. *Journal of Seismology, 21,* 1277–1284.

Beresnev, I. A. (2017b). Simulation of near-fault high-frequency ground motions from the representation theorem. *Pure and Applied Geophysics, 174,* 4021–4034.

Beresnev, I. A. (2019a). Interpretation of kappa and $f_{\max}$ filters as source effect. *Bulletin of the Seismological Society of America, 109,* 822–826.

Beresnev, I. A. (2019b). Reply to "Comment on "Interpretation of kappa and f_{max} filters as source effect" by Igor A. Beresnev" by Arthur Frankel. *Bulletin of the Seismological Society of America, 109,* 2764–2766.

Beresnev, I. A., & Atkinson, G. M. (1997). Modeling finite-fault radiation from the ω^n spectrum. *Bulletin of the Seismological Society of America, 93,* 67–84.

Boore, D. M., & Joyner, W. B. (1978). The influence of rupture incoherence on seismic directivity. *Bulletin of the Seismological Society of America, 68,* 283–300.

Graves, R. W., & Pitarka, A. (2010). Broadband ground-motion simulation using a hybrid approach. *Bulletin of the Seismological Society of America, 100,* 2095–2123.

Infantino, M., Mazzieri, I., Özcebe, A. G., Paolucci, R., & Stupazzini, M. (2020). 3D physics-based numerical simulations of ground motion in Istanbul from earthquakes along the Marmara segment of the North Anatolian fault. *Bulletin of the Seismological Society of America, 110,* 2559–2576.

Madariaga, R. (1977). High-frequency radiation from crack (stress drop) models of earthquake faulting. *Geophysical Journal of the Royal Astronomical Society, 51,* 625–651.

Madariaga, R. (1983). High frequency radiation from dynamic earthquake fault models. *Annales Geophysicae, 1,* 17–23.

Rodgers, A. J., Pitarka, A., Pankajakshan, R., Sjögreen, B., & Petersson, N. A. (2020). Regional-scale 3D ground-motion simulations of M_w 7 earthquakes on the Hayward fault, northern California resolving frequencies 0–10 Hz and including site-response corrections. *Bulletin of the Seismological Society of America, 110,* 2862–2881.

Shi, Z., & Day, S. M. (2013). Rupture dynamics and ground motion from 3-D rough-fault simulations. *Journal of Geophysical Research, 118,* 1122–1141.

Somerville, P., Irikura, K., Graves, R., Sawada, S., Wald, D., Abrahamson, N., Iwasaki, Y., Kagawa, T., Smith, N., & Kowada, A. (1999). Characterizing crustal earthquake slip models for the prediction of strong ground motion. *Seismological Research Letters, 70,* 59–80.

Wells, D. L., & Coppersmith, K. J. (1994). New empirical relationships among magnitude, rupture length, rupture width, rupture area, and surface displacement. *Bulletin of the Seismological Society of America, 84,* 974–1002.

(Received October 16, 2020, revised March 10, 2021, accepted March 13, 2021, Published online April 12, 2021)